PAPER

Neuronal adhesion, proliferation and differentiation of embryonic stem cells on hybrid scaffolds made of xanthan and magnetite nanoparticles

To cite this article: Talita Glaser *et al* 2015 *Biomed. Mater.* **10** 045002

Biomedical Materials

PAPER

Neuronal adhesion, proliferation and differentiation of embryonic stem cells on hybrid scaffolds made of xanthan and magnetite nanoparticles

RECEIVED
1 December 2014

REVISED
13 April 2015

ACCEPTED FOR PUBLICATION
19 May 2015

PUBLISHED
8 July 2015

Talita Glaser[1], Vânia B Bueno[2], Daniel R Cornejo[3], Denise F S Petri[2] and Henning Ulrich[1]

[1] Departamento de Bioquímica, Instituto de Química, Universidade de São Paulo, Av. Prof. Lineu Prestes 748, 05508-000, São Paulo, SP, Brazil
[2] Departamento de Química Fundamental, Instituto de Química, Universidade de São Paulo, Av. Prof. Lineu Prestes 748, 05508-000, São Paulo, SP, Brazil
[3] Instituto de Física, Universidade de São Paulo, São Paulo, Brazil

E-mail: dfsp@iq.usp.br, dfsp@usp.br and henning@iq.usp.br

Keywords: stem cells, scaffolds, magnetic nanostructures

Supplementary material for this article is available online

Abstract

Hybrid scaffolds made of xanthan and magnetite nanoparticles (XCA/mag) were prepared by dipping xanthan membranes (XCA) into dispersions of magnetic nanoparticles for different periods of time. The resulting hybrid scaffolds presented magnetization values ranging from 0.25 emu g^{-1} to 1.80 emu g^{-1} at 70 kOe and corresponding iron contents ranging from 0.25% to 2.3%, respectively. They were applied as matrices for *in vitro* embryoid body adhesion and neuronal differentiation of embryonic stem cells; for comparison, neat XCA and commercial plastic plates were also used. Adhesion rates were more pronounced when cells were seeded on XCA/mag than on neat XCA or plastic dishes; however, proliferation levels were independent from those of the scaffold type. Embryonic stem cells showed similar differentiation rates on XCA/mag scaffolds with magnetization of 0.25 and 0.60 emu g^{-1}, but did not survive on scaffolds with 1.80 emu g^{-1}. Differentiation rates, expressed as the number of neurons obtained on the chosen scaffolds, were the largest on neat XCA, which has a high density of negative charge, and were smallest on the commercial plastic dishes. The local magnetic field inherent of magnetite particles present on the surface of XCA/mag facilitates synapse formation, because synaptophysin expression and electrical transmission were increased when compared to the other scaffolds used. We conclude that XCA/mag and XCA hydrogels are scaffolds with distinguishable performance for adhesion and differentiation of ESCs into neurons.

1. Introduction

Neurodegenerative diseases affect at least 1% of people worldwide and cause general disabilities and high costs to the health system [1]. Stem cell therapies for recovery of neuronal loss is a promising strategy due to these cells having the capabilities of self-renew and differentiation into specialized tissue types. Clinical studies using stem cells and fetal mesencephalic tissue in Parkinson's disease are currently in progress [2–6]. The results of some of these studies showed that stem cells can graft into the brain, become functionally integrated, and promote regeneration. In this regard, mouse embryonic stem cells (ESC) revealed the best results for re-innervation and restoration of dopamine release. Nevertheless, dysfunctional grafts led to dyskinesia after transplantation. For a hypoxia–ischemia model [7], which is a common cause of neurological disability in adults and children, even the most capable cells needed intrinsic organization and a scaffold to guide restructuring. In view of that, successful cell replacement therapy must fulfill some requirements, such as that neuronal-differentiated cells must reveal similar phenotypes, including molecular, morphological, and electrophysiological characteristics, and axonal growth must be specified from grafts to correct sites in the brain or spinal cord.

Artificial scaffolds produced by combining materials chemistry, elasticity, and topology might stimulate cell proliferation and differentiation for regenerative applications [8]. Polymeric scaffolds are potential candidates for meeting these requirements. The first

report on scaffolds for stem cells during spinal cord repair described the use of a blend composed of poly(lactic-co-glycolic acid) (PLGA) and a block copolymer of poly(lactic-co-glycolic acid)-polylysine; the advantage of PLGA is its fast (up to 60 d) degradation [9]. Neural stem cells plated on poly(glycolic acid) scaffolds were implanted around the brain infarction cavity with the result being that grafted cells were attached, impregnated, and migrated throughout this polymer, partially recovering the brain from injury [7]. Electrospun fibrous polyurethane scaffolds were successfully applied for the *in vitro* differentiation of human ESC [10]. The presence of magnetic nanoparticles in polymeric matrices particularly stimulates cell proliferation [11]. For instance, polycaprolactone scaffolds containing magnetic nanoparticles induced more active osteogenic differentiation and improved cellular mineralization in comparison to pure caprolactone [12]. Bone repair and regeneration were achieved with scaffolds composed of hydroxyapatite, collagen, and magnetic nanoparticles [13]. Myoblast cells labeled with magnetic nanoparticles, used as the basis for artificial tissue construction, formed multilayered cell sheets in the presence of an external magnetic field [14].

In the present work, xanthan gum based scaffolds were prepared to be applied as supports for *in vitro* adhesion and neuronal differentiation of ESC. Xanthan gum was chosen because it is a biodegradable and biocompatible polysaccharide approved by the FDA (Fed. Reg. 345376) [15]. Xanthan chains can form chemical networks by reacting with citric acid, an efficient nontoxic crosslinker for polysaccharides [16–18]. Hybrid scaffolds of xanthan and nanohydroxyapatite or its equivalent strontium substituted were suitable for osteoblast growth and induced high alkaline phosphatase activity [19]. Dipping the xanthan networks for 10 seconds in an aqueous dispersion of magnetite (Fe_3O_4) nanoparticles led to hybrid scaffolds with magnetization of 0.02 emu g^{-1} at 1000 Oe and iron content of 0.4 ± 0.1 wt%, which served as outstanding scaffolds for fibroblasts proliferation [20]. In the present study hybrid scaffolds made of xanthan and magnetite nanoparticles (XCA/mag) were prepared with different magnetization values by dipping the xanthan membranes for different periods of time into the aqueous ferrofluid. XCA/mag scaffolds, neat xanthan scaffolds (XCA), and commercial plastic dishes were used for *in vitro* neuronal differentiation of ESC. ESC that previously differentiated into neural precursor cells underwent neuronal differentiation such as those observed under standard *in vitro* conditions. Only XCA/mag scaffolds with iron content lower than 1 wt% were used because scaffolds with higher amounts of iron were toxic. Cells attached better to XCA/mag than to neat XCA. Moreover, cells differentiated on XCA/mag showed increased membrane potential amplitudes on depolarization with KCl, indicating successful synapse formation.

2. Materials and methods

2.1. Scaffolds preparation and characterization

The synthesis of magnetite is described in detail elsewhere [20]. $FeCl_3.6H_2O$ and $FeCl_2{\cdot}4H_2O$ (both from Labsynth, Diadema, Brazil) at 0.1 mol l^{-1} and 0.05 mol l^{-1}, respectively, were vigorously mixed in an IKA Vortex mixer Genius 3 (IKA Werke GmbH & Co., Staufen, Germany). NH_4OH (25 % V/V) was added to the system under stirring until the solution achieved pH 9. Nitrogen gas was bubbled directly into the media prior to reaction for removal of oxygen. Then, the system was placed in a water bath at (24 ± 1) °C, in which the sonotrode MS7 with acoustic power density of 130 W cm^{-2} coupled to the ultrasonic processor Hielscher UP100H (Hielscher Ultrasonics GmbH, Teltow, Germany) was immersed. The sonotrode was kept outside of the reaction flask to avoid contamination by Ti particles stemming from the device. The sonotrode operated for 10 min. The temperature inside and outside of the reaction flask remained at 24 ± 1 °C. Prior to use, the dispersion containing the magnetite (Fe_3O_4) particles was neutralized. Magnetic particles were separated by centrifugation at 1200*g* during 10 min. They were redispersed in MilliQ water and again separated. This rinsing process was repeated three times to remove the excess of reactants. One should note that no stabilizer was added to the magnetic nanoparticles dispersions. The concentration of magnetite in the dispersion was determined by gravimetric analyses as 48 ± 2 g l^{-1}. The magnetic nanoparticles presented an isoelectric point of 6.5 ± 0.1 and the nearly superparamagnetic behavior at room temperature, with coercivities less than 20 Oe in all samples [20].

Xanthan gum (Mv ~ 10^6 g mol^{-1}, degree of pyruvyl = 0.38, degree of acetyl = 0.41; CP Kelco, Atlanta, GA) was dissolved in water at 6 g l^{-1} in the presence of citric acid at 0.3 g l^{-1}. The solutions were homogenized with an Ika Turrax® (IKA Werke GmbH & Co., Staufen, Germany) stirrer at 18 000 rpm for 3 min and submitted to centrifugation for 5 min at 1014 g to remove air bubbles prior to casting. The solution of xanthan and citric acid was cast into plastic molds and allowed to dry in an oven at 45 °C overnight to form films. Crosslinking was achieved by heating the dried films at 165 °C for 7 min. The resulting xanthan networks were swollen in water at 70 °C for 24 h to remove sol fraction and dried at 45 °C for 24 h. More details about the crosslinking reactions can be found elsewhere [17]. The resulting cross-linked xanthan films were 80 ± 5 μm thick, stable in the pH range of 2 to 9, and after swelling in water (under equilibrium conditions) their mass increased up to 27 times compared to its original dried mass [17]. The xanthan films were immersed in the magnetic nanoparticle dispersions at pH 6 and 24 ± 1 °C during 10 s, 1 min, 5 min, 1 h, or 24 h. At this pH, the magnetic particles are positively charged [20]. After that, the films were removed and rinsed in MilliQ water for 20 s.

This process was repeated three times more to remove particles weakly attached to polymeric matrix. Details about hybrid scaffold preparation can be seen in the movie at www.youtube.com/watch?v=PhTn2M_NRF8&index=2&list=UUqVKEBUzLfSAoMIzF8r9VTA). The xanthan films impregnated with magnetic nanoparticles were gently dried with paper tissues, freeze-dried for inductively coupled plasma atomic emission spectroscopy (ICP-AES) analyses, or dried in the oven overnight at 50 ± 1 °C for analyses with superconducting quantum interference device (SQUID) magnetometer (model MPMS; Quantum Design, USA; details are in online supplementary information SI1; stacks.iop.org/BMM/10/045002/mmedia).ICP-AES analyses performed with Spectro Smart Analyzer Vision equipment (SPECTRO Analytical Instruments GmbH, Germany) yielded the amount of iron in the magnetite-impregnated XCA films. Freeze-dried XCA networks were analyzed (after gold coating by sputtering) by scanning electron microscopy (SEM) in a Jeol microscope FEG7401F equipped with a field-emission gun. The hybrid XCA/mag scaffolds were analyzed by FEI Inspect F50 high resolution SEM. Samples were prepared by tearing small pieces of composite films already used in the magnetization measurements. The samples moved toward the electromagnetic lens during the analyses; for this reason, the small slivers must be sandwiched within oyster TEM grids to avoid sample movement. Scanning electron images were then acquired without any coating in transmission (STEM) at the edges of the film's lower surface. More details about the experimental procedure can be found elsewhere [20].

Controls incorporating non-magnetic nanoparticles in the XCA scaffolds were included to evaluate the effects mediated by the magnetic nanoparticles. The controls, coded as XCA/HA, were XCA scaffolds with hydroxyapatite particles at 10 wt%. The preparation and characterization of this type of scaffolds are described elsewhere [19].

2.2. Cell culture and differentiation of E14Tg2A mouse embryonic stem cell

The feeder cell-independent E14Tg2A embryonic stem [21] was kindly provided by Dr Deborah Schechtman, Institute of Chemistry, University of São Paulo, Brazil. Undifferentiated cells were cultured as described by Fornazari and coworkers [22]. For neuronal differentiation, 5×10^6 cells were cultured in 90 mm × 15 mm non-adherent plates in DMEM supplemented with 20% FBS, 1% non-essential amino acids, and 0.1mM β-mercaptoethanol for 48 h to induce embryoid body formation. Following substitution of the culture medium, cells were maintained in suspension for another 4 d in the presence of 5μM retinoic acid. Embryoid bodies were seeded in 125 mm adherent cell culture flasks with tissue advanced treatment (Greiner Bio One, Frickenhausen, Germany) and grown for another 4 or 12 d in DMEM/F12 medium supplemented with 1% Bottenstein's N-2 formulation (Life Technologies, USA) and b-FGF 100 ng ml^{-1} (Sigma-Aldrich, USA). The procedure is schematically depicted in online supplementary information SI2 (stacks.iop.org/BMM/10/045002/mmedia).

2.3. Embryoid body adhesion assay

To evaluate the effects of the different scaffolds on the cell adhesion, 50 embryoid bodies (EBs) on the day of differentiation were seeded on the scaffolds in p35mm dishes for each experiment performed in duplicate. Following 24 h of seeding, EBs were collected in the presence of PBS containing 5mM EDTA and then resuspended in 1 ml of Dulbecco's phosphate buffered saline (DPBS) solution. EB quantities were determined with a Neubauer chamber (0.100 mm depth, 0.0025 mm^2 area) on an inverted microscope (Axiovert 200; Zeiss, Aalen, Germany). Images were produced with a Nikon DMX1200F camera, equipped to the microscope, and further processed with the Image J image analysis program. To evaluate the effect of the external magnetic field (EMF) on cell adhesion and proliferation, neodymium magnet (0.4 T) arrays were placed under the culture plates containing the scaffolds (see online supplementary information SI3; stacks.iop.org/BMM/10/045002/mmedia).

2.4. Cell viability assay

To evaluate the effects of the different types of scaffolds on the cell viability, 50 EBs were seeded on the scaffolds in p35 mm dishes for each experiment performed in duplicate. Following 24 h of seeding, EBs were collected in the presence of PBS containing 5mM EDTA and then resuspended in 1 ml of DPBS solution. An aliquot of 10 µl was mixed with 0.08% Trypan Blue dye solution and cell quantities were determined with a Neubauer chamber (0.100 mm depth, 0.0025 mm^2 area) on an inverted microscope (Axiovert 200; Zeiss, Aalen, Germany). Stained and unstained cells represent dead and healthy cells, respectively; cell viability should be at least 95% for healthy log-phase cultures [23].

2.5. Determination of the progress of differentiation by flow cytometry analysis

Efficiencies of the differentiation progress were measured by flow cytometry population analysis of immunostaining against neuronal markers TUJ1 and MAP2, labeling young and mature neurons, respectively. For this purpose, cells were fixed for 30 min with a 4% paraformaldehyde solution, washed in PBS, and blocked in PBS supplemented with 2% fetal bovine serum and 0.1% Triton-X100. The cells were then exposed for 1 h to mouse anti-TUJ1 (Sigma-Aldrich, St. Louis, MO; 1 : 700 dilution) or rabbit anti-MAP2 (cell signaling, Danvers, MA; 1 : 500 dilution). The cells were incubated for 45 min with Alexa Fluor 488 anti-rabbit or Alexa Fluor 647 anti-mouse secondary antibodies (Life Technologies, Grand Island, NY; 1 : 1000 dilution, respectively). Cells that were not marked with the

primary antibodies were used as negative control and were used to set gates at FlowJo software (Flowjo LLC, USA). The percentage of marked cells was measured by using a flow cytometer (Attune, Life Technologies). Alexa Fluor 488 was excited by a 488 nm blue laser and its emission was captured through a 530/30 band pass filter. Alexa Fluor 555 was excited by a 488 nm blue laser and its emission was captured through a 574/26 band pass filter. Alexa Fluor 647 was excited by a 638 nm red laser and its emission was captured through a 660/20 band pass filter.

2.6. Microfluorimetric measurements of alterations in the membrane potential

Changes in membrane potential were determined by microfluorimetry using the FlexStation III (Molecular Devices Corp., Sunny Valley, CA), following the instructions of the manufacturer. Briefly, EBs collected on day 6 of differentiation were seeded in 96-well black microplates with clear bottoms at a concentration of 2 EBs/well in 100 µl of cell culture medium. Cells were incubated for 60 min and 37 °C with the FlexStation membrane potential Assay Kit (Molecular Devices Corp.) containing 2.5mM probenecid in a final volume of 200 µl per well. Fluorescence of samples was excited at 488 nm, and fluorescence emission was detected by the 540–590 nm Band Pass Emission FLIPR Filter. Samples were read at 1 s intervals for a period of 120 s. Following 30 s of monitoring basal fluorescence intensities were used as a measure of the membrane potential levels of resting cells. A depolarizing agent (KCl at 10–100mM concentrations) was added to the cells. Responses to agent addition were determined as peak fluorescence minus the basal intensity. Fluorescence intensity was analyzed using the SoftMax2Pro software (Molecular Devices Corp.). Data were expressed as mean values ± standard errors (S.E.).

2.7. Cell proliferation evaluation by flow cytometry analysis

Cell proliferation was measured following fixation with ice-cold 75% ethanol for 10 min, washing with PBS, and blocking with 2% fetal bovine serum 0.1% Triton-X solution in PBS for 30 min. After washing with PBS, cells were incubated for 1 h with rabbit anti-Ki67 antibody (Billerica, MA; 1:500 dilution), which is a marker for proliferating cells. Alexa Fluor 488 secondary antibody (Life Technologies) was used at 1:1000 dilution. Alexa Fluor 488 was excited by a 488 nm blue laser and emission was captured through a 530/30 nm filter.

2.8. Immunofluorescence staining assay

To analyze neuron morphology during the differentiation progress, we immunolabeled the cells with neuronal markers as TUJ1 (young neurons) and performed fluorescence microscopy. For this purpose, the cells were grown and induced to differentiate on rounded coverslips (1 cm diameter) and were fixed with a 4% paraformaldehyde solution for 30 min, washed in PBS, and blocked with 5% fetal bovine serum 0.1% Triton-X solution in PBS for 30 min. The cells were then incubated in mouse anti-TUJ1 (Sigma Aldrich, USA; 1:1000 dilution) or mouse anti-Synaptophysin (Axyll, Bethesda, MD; 1:50 dilution), or rabbit anti-ISL1 (GeneTex, Irvine, CA; 1:200 dilution) or rabbit anti-Pax6 (GeneTex; 1:200 dilution) antibodies for 18 h. The cells were incubated for 45 min with the Alexa Fluor 488 anti-mouse secondary antibody (Life Technologies; 1:1000 dilution). Cells that were not marked with the primary antibodies were used as negative control. Cell nuclei were stained with 0.1% of 4′,6-diamidino-2-phenylindole (DAPI), and then the slides were mounted with Vectashield (Vector Laboratories, Burlingame, CA) and examined on an Axiovert 200 epifluorescence microscope (Zeiss) equipped with a Nikon DMX1200F camera and Metamorph image analysis program. Alexa Fluor 488 was excited by a 488 nm blue light and its emission was captured through a 530/30 band pass filter.

2.9. Statistical analysis

Comparisons between experimental data were performed using one-way analysis of variance following the Bonferroni *post hoc* test using GraphPad Prism 5.0 software (GraphPad Software, La Jolla, CA). Criteria for statistical significance were set at $p < 0.05$ (*), $p < 0.01$ (**), or $p < 0.001$ (***).

3. Results and discussion

XCA/mag scaffolds were prepared by immersing XCA films into an aqueous dispersion of magnetic nanoparticles for 10 s, 1 min, 5 min, 1 h, or 24 h. The magnetization (σ) and the content of iron in the resulting materials increased exponentially with the immersion time, as presented in figures 1(A) and (B), respectively. XCA/mag with magnetizations of 0.25 emu g^{-1} (10 s), 0.6 emu g^{-1} (1 h = 3600 s), and 1.8 emu g^{-1} (24 h = 86 400 s), coded as XCA/mag10S, XCA/mag1H, and XCA/mag24H, respectively, were chosen as scaffolds to evaluate the effects of magnetization on the progress of proliferation and neuronal differentiation. As control experiments, neat XCA (0 emu g^{-1}) and commercial plastic dishes were also tested. At room temperature (300 K) the coercivity determined for all samples was on the order of 16 Oe (inset figure 1(A)); such a low value is characteristic of superparamagnetic particles. The iron content increased with immersion time of XCA into magnetite nanoparticle dispersions (figure 1(B)) and the films became browner, corroborating with the magnetization increased observed in figure 1(A). XCA networks presented micrometric pores, and the mean diameter of magnetic particles ranged from 6 nm to 17 nm (online supplementary information SI4; stacks.iop.org/BMM/10/045002/mmedia). Most particles were observed on the network uppermost layers. Although the pores are large enough for the diffusion of

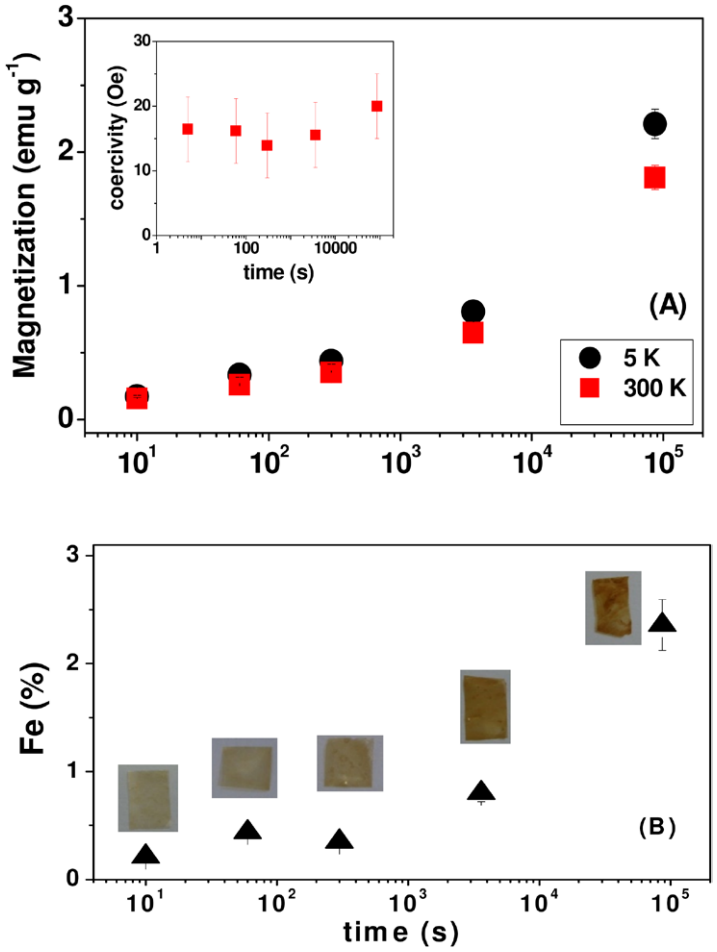

Figure 1. (A) Magnetization recorded at 5 K (black circles) and 300 K (red squares) with maximum magnetic field of 70 kOe and coercivity measured at 300 K (inset, black triangles) and (B) iron content determined by ICP-AES analyses and photographs taken for XCA/mag samples prepared by immersing XCA films into magnetite dispersion for different periods of time.

nanoparticles to the network interior, the electrostatic attraction between xanthan chain carboxylate groups and positively charged patches on magnetic particles might have driven the particles adsorption just after the first contact with the network surface (online supplementary information SI4; stacks.iop.org/BMM/10/045002/mmedia). Moreover, the chance to diffuse to the deeper layers was small because of the short period of contact.

Scaffolds for cell therapy must show good adherence to cells. In view of this, first the cell adhesion onto bare XCA and XCA/mag films was evaluated. For cell adhesion experiments embryonic stem cells (ESC) were pre-differentiated into neural precursor cells by embryoid body suspension culture, as described elsewhere [24], and then seeded for comparison of adhesion rates onto XCA, XCA/mag scaffolds, and commercial plastic dishes. XCA/mag24H scaffolds with 2.3 wt% Fe and magnetization of 1.8 emu g^{-1} were not suitable for neural cell culture because most cells died after 2 d. The cytotoxicity of superparamagnetic particles depends not only on the concentration but also on particle size, shape, and type of coating, and on the administrative route in the case of *in vivo* tests [25]. However, significant amounts of EBs adhered onto XCA/mag10S and XCA/mag1H films with magnetizations of 0.25 emu g^{-1} and 0.6 emu g^{-1} at rates of 20-fold and 15-fold, respectively, which is larger than that observed for neat XCA or plastic dish controls, as presented in figures 2(A) and (B). Furthermore, using the XCA/mag scaffolds, more cells migrated from the EB (figures 2(A-III) and (A-IV)) to finally differentiate into neurons when compared to the further experimental conditions. For quantification of adhered cells 1 d after seeding, scaffolds were gently rinsed for removal of cells in suspension, followed by gentle detachment and counting of EBs (figure 2(B)). EBs showed significantly higher rates of attachment onto XCA/mag scaffolds (0.25 and 0.6 emu g^{-1}) than onto neat XCA or control plastic dishes. Similar effects were observed for the proliferation of fibroblasts [20]; fibroblast proliferation was larger on XCA/mag10s (0.25 emu g^{-1}) than on neat XCA.

In a previous work [20], an external static magnetic field (ESMF) of 0.4 T positioned beneath the culture plates increased the proliferation of fibroblasts plated on neat XCA or XCA/mag10S. Similarly, myogenic cell differentiation was stimulated by the presence of magnetic nanoparticles and external magnetic field [14]. To extend this effect to neurogenesis, EBs pre-differentiated for 6 d were seeded onto XCA/mag1H

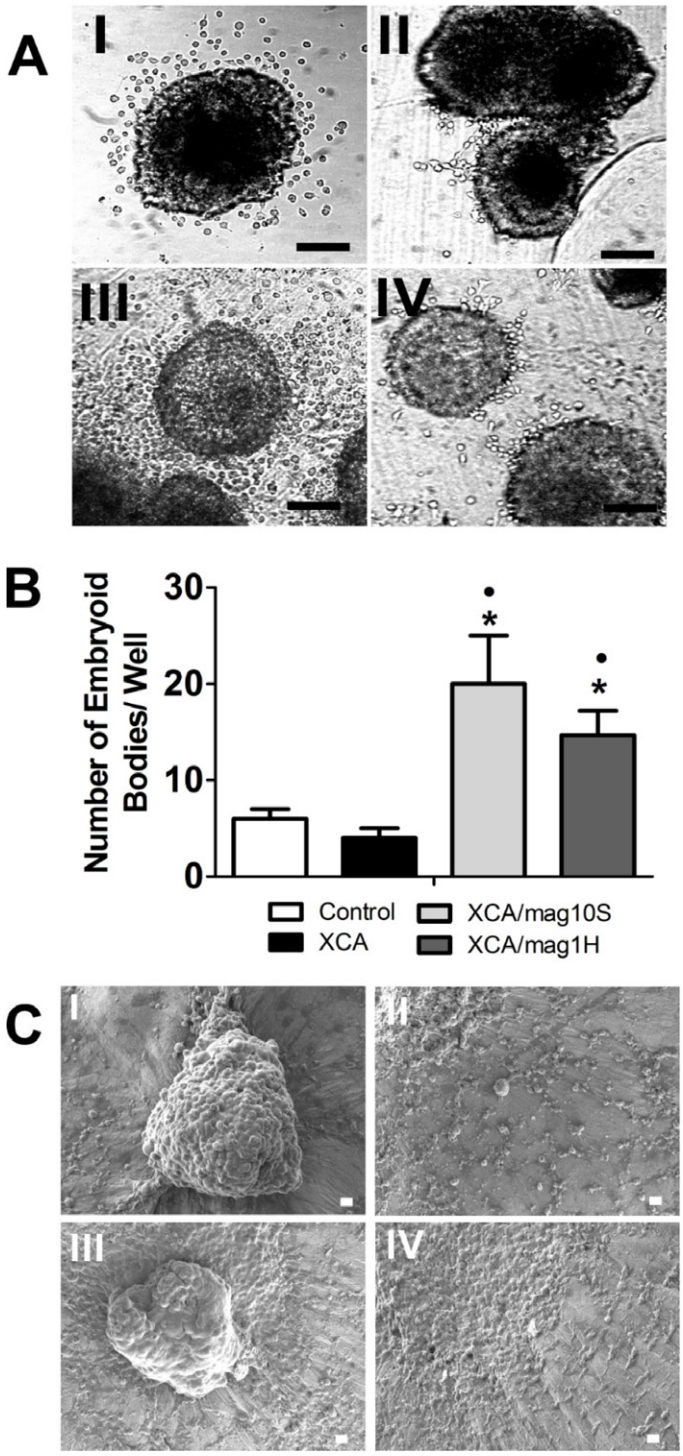

Figure 2. Cell adhesion and migration on xanthan based scaffolds during neural differentiation of ESC. (A) ESCs were induced to neural differentiation by embryoid body formation and all trans-retinoic acid application and then seeded onto commercial plastic dishes (I), neat XCA (II), XCA/mag10S (III), and XCA/mag1H (IV) scaffolds. (B) Counting of EBs attached to plastic dishes (control), neat XCA, XCA/mag10S, and XCA/mag1H. ANOVA following Bonferroni *post hoc* test $*p \leq 0.05$ compared to control. ● $p \leq 0.05$ compared to XCA. (C) Scanning electron microscopy for EBs differentiated for 14 d and seeded onto XCA/mag1H scaffolds. Cells cultured with ESMF of 0.4 T (I and II) and without ESMF (III and IV) onto XCA/mag1H. EB (I and III) and migrating cells (II and IV). Scale bar = 10 μm.

scaffolds and cultured in the absence and in the presence of ESMF (0.4 T). SEM images obtained for cells cultivated onto XCA/mag1H scaffolds with (figures 2(C-I) and (C-II)) and without (figures 2(C-III) and (C-IV)) ESMF provided evidence for EB attachment onto XCA/mag1H and neural progenitor cell migration with a radial pattern. Thus, morphological differences did not result from ESMF, and cell adhesion rates were also not affected by ESMF. Although various cell types, including fibroblasts [20], myoblasts [14], and osteoblasts [26], were affected by ESMF in their proliferation rates, neural cells were indifferent to ESMF stimulation. A possible explanation for this effect could be that the local electromagnetic field

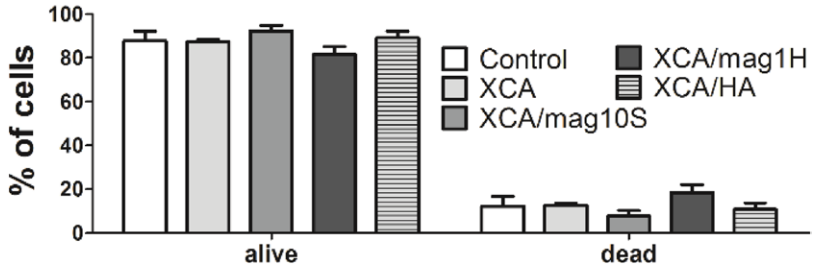

Figure 3. Cell viability of ESCs differentiated on tissue culture dishes (control), neat xanthan (XCA), XCA/mag10S, XCA/mag1H, and XCA/HA. XCA/HA refers to XCA scaffolds with hydroxyapatite particles at 10 wt%. Dissociated cells were stained with trypan blue dye for quantification of viability rates. Stained cells were dead and unstained were alive.

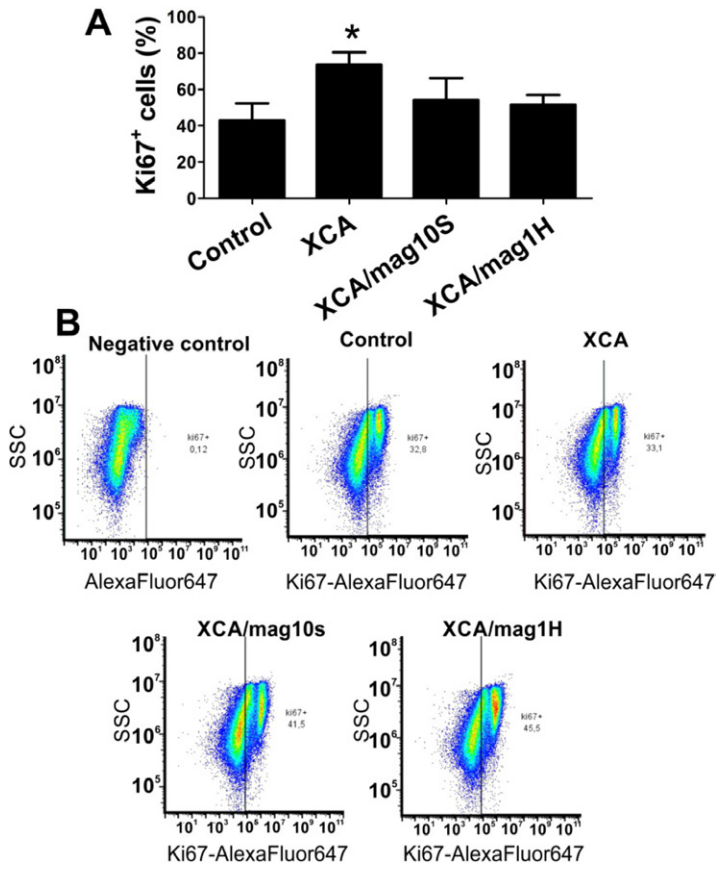

Figure 4. Cell proliferation during ESC neuronal differentiation on xanthan based scaffolds. EBs pre-differentiated for 14 d were seeded onto commercial plastic dishes. Following 14 d of culture, XCA scaffolds were immunostained for Ki67 expression and analyzed by flow cytometry as described in the methods section. Control (commercial plastic dish), neat XCA, XCA/mag10S, and XCA/mag1H. (A) Percentage of Ki67-positive immunostained cells. (B) Density plots showing gates and population distribution. Side-scattered light (SSC) and fluorescence intensity of Alexafluor 647 were analyzed. Small inserted graphs show the negative control used for setting gates.

inherent to the presence of magnetite nanoparticles was already enough to stimulate neural cell migration and differentiation.

Cell viability tests were performed for the different scaffolds. The data are presented in figure 3. They showed that none of the scaffolds tested was toxic for the cells. XCA/mag1H presented the highest cell death of approximately 19%. Elevations in cell death levels are expected as the dose of magnetic nanoparticles increases, mainly due to the release of iron ions, which can work as oxidative free radicals [27].

During the regeneration process, cells must be able to proliferate to recover the nervous system. The highest percentage of Ki67-positive cells, expressed during cell cycle progression, was observed for cells on neat XCA (figure 4). No statistically significant alterations were noted in percentages of Ki67-positive cells seeded onto control (commercial plastic dish), XCA/mag10S, and XCA/mag1H supports (figure 4), indicating that cells were still able to proliferate.

Neurogenesis of ESC might be detected by the occurrence of cells expressing neuronal marker

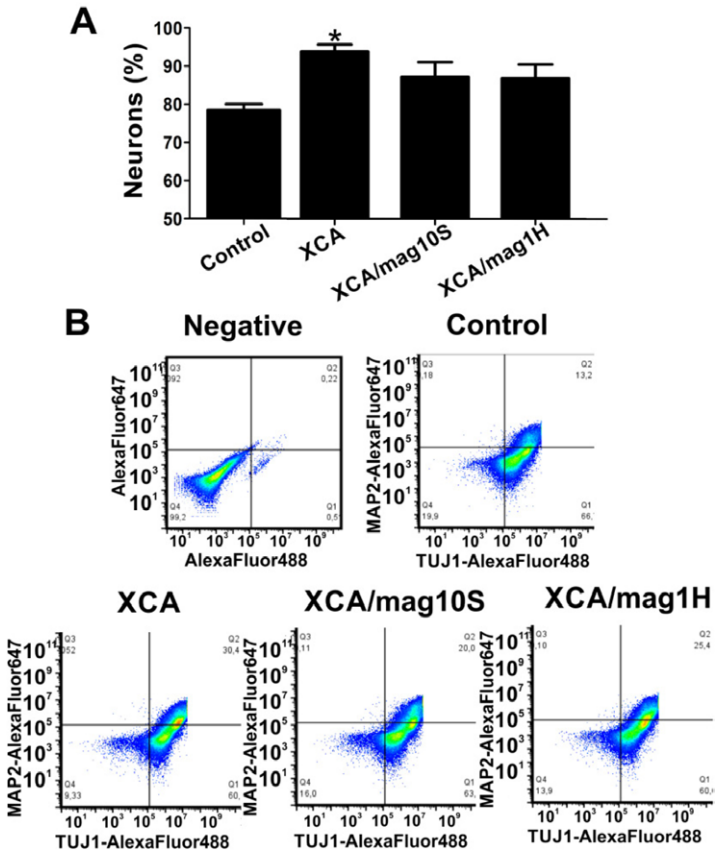

Figure 5. Neuronal differentiation efficiency. EBs differentiated for 14 d and seeded onto XCA scaffolds were immunostained for TUJ1 and MAP2, which are proteins expressed by young neurons and mature neurons, respectively, and further analyzed by flow cytometry as described in the methods section. (A) Percentage of all TUJ1- and MAP2-positive immunostained cells were summed and plotted. (B) Density plots showing gates and population distribution. Fluorescence intensities of Alexafluor 647 and Alexafluor 488 emissions were quantified. Experiments were performed as three independent experiments (* $p < 0.05$, versus control).

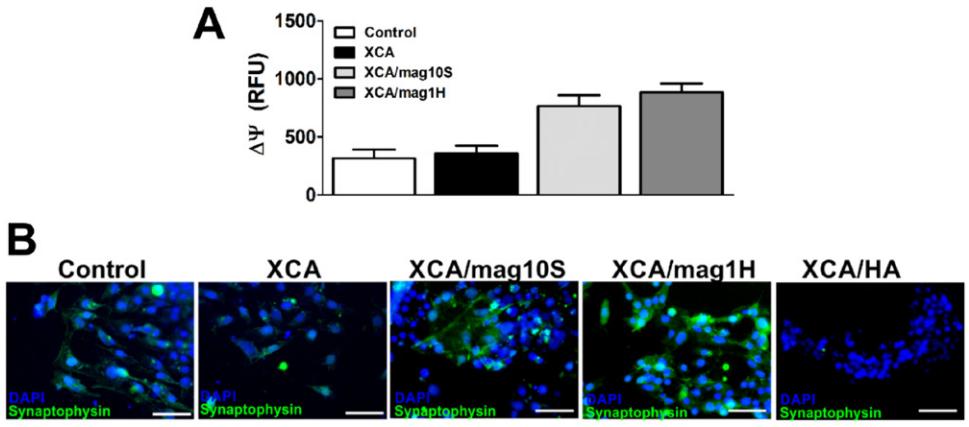

Figure 6. Neuronal differentiation of embryonic stem cells and macrostructure formation onto scaffolds. (A) For measurement of changes in membrane potential, EBs were seeded on black 96 well plates with clear bottoms with or without XCA scaffolds. Changes in the membrane potential were measured by microfluorimetry upon treatment with the depolarizing KCl. Control (commercial plastic dish), neat XCA, XCA/mag10S, and XCA/mag1H are described. (B) Fluorescence microscopy images of previously differentiated ESC onto tissue culture dish (control), neat xanthan (XCA), XCA/mag10S, XCA/mag1H, and XCA/HA immunostained for expression of synaptophysin, a synapse protein marker. Nuclei: DAPI (blue) and synaptophysin (green). Scale bar = 100 μm.

proteins, including TUJ1 and MAP2. Figures 5(A) and (B) show that cells differentiated on neat XCA revealed a statistically significant increase in the percentage of neurons in comparison to XCA/mag10S or XCA/mag1H or plastic dishes control, as judged by TUJ1 expression and MAP2 expression by flow cytometry, indicating that neat XCA scaffolds promote neuronal differentiation. Moreover, under KCl

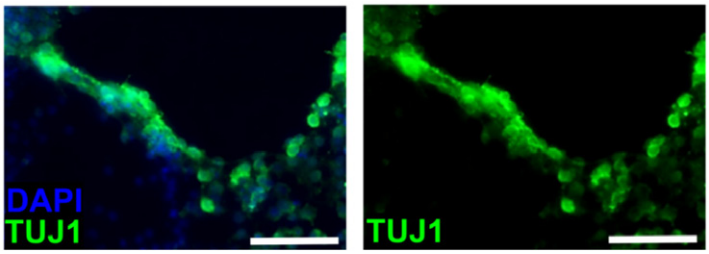

Figure 7. Neuronal differentiation of embryonic stem cells and macrostructure formation onto XCA/mag1H. Fluorescence microscopy images of previously differentiated ESC onto XCA/mag1H and immunostained for expression of TUJ1, marking neurons. There are some small neuron arrays similar to neural bundles. Nuclei: DAPI (blue) and TUJ1 (green). Scale bar = 100 μm.

depolarization, alterations of the membrane potential were not different for cells plated onto the plastic dish or neat XCA (figure 6(A)), indicating that polymers do not affect the capability of neurons to form electrical synapses. Nevertheless, alterations of the membrane potential under KCl depolarization, measured as an increase in fluorescence of the lipid dye, doubled in comparison to neat XCA or plastic dish, when cells were seeded onto XCA/mag10S or XCA/mag1H scaffolds, indicating that the presence of magnetic nanoparticles in the scaffolds gave rise to neurons with higher responsiveness to electrical stimuli and supposedly increased synaptogenesis (figure 6(B)), as confirmed by immunostaining against the synapse-specific synaptophysin.

Immunofluorescence assay allowed to observe the formation of some macrostructures composed of neurons differentiated from cells seeded onto XCA/mag1H scaffolds (figure 7). These structures may resemble neuron bundles, suggesting that this scaffold is potentially interesting for the comprehension of nerve growth and differentiation.

Moreover, the scaffolds enabled cells to differentiate to both motor and sensory neurons, as seen by the immunostaining of ISL1, a transcription factor related to motor neuron differentiation (figure 8(A)), and Pax6, a transcription factor related to motor neuron differentiation (figure 8(B)). Fluorescence intensities of nuclear ISL1 and Pax6 were quantified and normalized using DNA staining intensity (figures 8(C) and (D)). The results clearly indicate that XCA/mag1H facilitated the ESC differentiation into sensory neurons, because Pax6 expression was increased in this condition.

The physical chemical properties of scaffolds, such as porosity, elasticity, hydrophilicity, and roughness, play an important role in the cell response. The main difference between XCA/mag and XCA/HA scaffolds is that the former has magnetic properties and the latter is diamagnetic. XCA/HA scaffolds were already successfully used as scaffolds for osteoblasts proliferation; however, the results in online supplementary material figure SI5 (stacks.iop.org/BMM/10/045002/mmedia) show that they are suitable for glial differentiation. However, the effects of XCA/mag scaffolds during differentiation were specific for neuronal phenotypes because the proportion of neural precursor cells and glia cells were not affected.

Magnetite and maghemite nanoparticles are naturally present in human brain tissue [28, 29]. Their formation involves the ferritin protein complex, which is responsible for the storage and release of iron. Ferritin can oxidize Fe(II) to Fe(III) as ferrihydrite ($5Fe_2O_3{\cdot}9H_2O$), which is stored in the protein core. When it is overloaded, the protein loses its oxidative function and this situation might favor the formation of biogenic magnetite [28]. In brains with neurodegenerative disorders, biogenic magnetite particles were found in larger concentrations than in normal brains. Recently, Dadras and coworkers [30] observed conformational changes of tubulin, a precursor of microtubules, in the presence of large amounts of magnetite. The authors of this article proposed that the local magnetic field inherent of magnetite particles affects axonal microtubules, generating electromagnetic fields by the movement of electrons along the axons in normal brain function. Such induction of electron current along microtubules would be disrupted in the presence of a large amount of magnetite and the transport of axonal neurotransmitters affected, causing neuronal disorders [30]. Corroborating our data, an excess of magnetite can lead to cell disorders (death, malfunction), whereas lower concentrations present benefits to neural cell function.

In the present work neat XCA and XCA/mag loaded with less than 1 wt% iron were used successfully as scaffolds for neuronal cell adhesion, proliferation, and differentiation. The main results can be summarized as follows.

- Cells responded similarly to scaffolds with magnetization of 0.25 and 0.60 emu g^{-1}.
- The amounts of EBs adhered to XCA/mag10S and XCA/mag1H films were larger than those observed for neat XCA or plastic dish controls.
- Cells proliferated on XCA, XCA/mag, and commercial plastic dishes in a similar way.

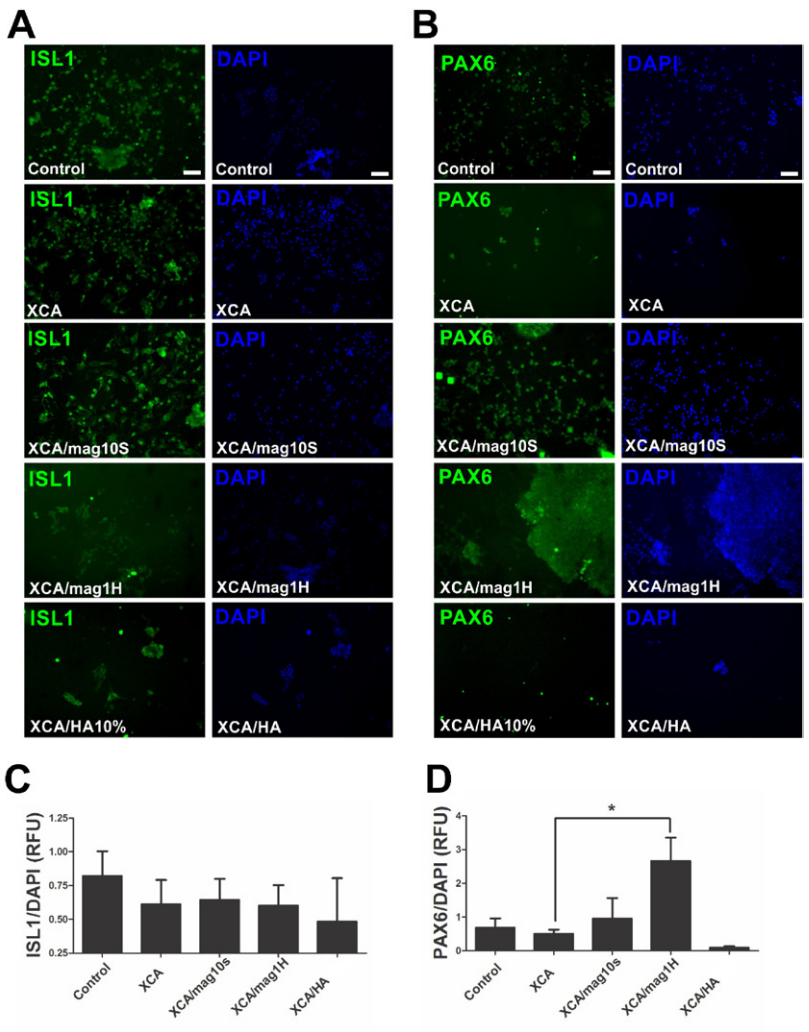

Figure 8. Differentiation of ESCs into motor or sensory neurons onto scaffolds. Fluorescence microscopy images of previously differentiated ESC onto tissue culture dish (control), neat xanthan (XCA), XCA/mag10S, XCA/mag1H, and XCA/HA immunostained for ISL1 expression, a transcription factor acting in motor neuron differentiation (A), or for Pax-6 expression, a transcription factor specific for sensory neuron differentiation (B). Respective quantification for ISL-1 (C) and Pax-6 (D) normalized using DNA staining levels (DAPI). Nuclei: DAPI (blue); ISL-1 or Pax-6 (green), $p < 0.05$. Scale bar = 100 μm.

- The differentiation was expressed as the number of neurons grown on the scaffolds. The largest amount of neurons was observed on neat XCA and the smallest amount was observed on the commercial plastic dishes. XCA is a hydrogel with a high density of negative charge [18], which provides an electrical field for adequate differentiation.
- Neurons grown onto XCA/mag scaffolds responded better to electrical stimuli. Electrons of the local magnetic field, inherent of magnetic particles, are suggested to contribute to ion translocation along the plasma membranes of axonal microtubes.

4. Conclusions

XCA and XCA/mag scaffolds are easy to prepare, biocompatible, and of low cost. In comparison to commercial plastic dishes, these scaffolds offer a suitable environment for *in vitro* neuronal cell attachment, proliferation, and differentiation. The combination of highly charged polymer network (XCA) and magnetite nanoparticles creates local electromagnetic fields, which stimulate these processes. Ultimately, such scaffolds might also benefit the delivery of the agents to speed the neuronal tissue regeneration processes.

Acknowledgments

This work was supported by research grants from Brazilian funding agencies Sao Paulo Research Foundation (FAPESP) Grants 2010/13034-2, 2010/51219-5, and 2012/50880–4; National Council for Scientific and Technological Development (CNPq) Grants 305178/2013-0 and 404663/2012–5 and Rede Nanobiotec CAPES; and Provost's Office for Research of the University of São Paulo, Grant number: 2011.1.9333.1.3 (NAPNA-USP), Brazil.

References

[1] de Lau L M and Breteler M M 2006 Epidemiology of Parkinson's disease *Lancet Neurol.* **5** 525–35

[2] Dunnett S B and Rosser A E 2014 Challenges for taking primary and stem cells into clinical neurotransplantation trials for neurodegenerative disease *Neurobiol. Dis.* **61** 79–89
[3] Lindvall O and Bjorklund A 2004 Cell therapy in Parkinson's disease *NeuroRx* **1** 382–93
[4] Lindvall O, Kokaia Z and Martinez-Serrano A 2004 Stem cell therapy for human neurodegenerative disorders-how to make it work. *Nat. Med.* **10** (Suppl.) S42–50
[5] Nery A A, Nascimento I C, Glaser T, Bassaneze V, Krieger J E and Ulrich H 2013 Human mesenchymal stem cells: from immunophenotyping by flow cytometry to clinical applications *Cytometry* **83A** 48–61
[6] Oliveira S L, Pillat M M, Cheffer A, Lameu C, Schwindt T T and Ulrich H 2013 Functions of neurotrophins and growth factors in neurogenesis and brain repair *Cytometry* **83A** 76–89
[7] Park K I, Teng Y D, Snyder E Y 2002 The injured brain interacts reciprocally with neural stem cells supported by scaffolds to reconstitute lost tissue *Nat. Biotechnol.* **20** 1111–17
[8] Murphy W L, McDevitt T C and Engler A J 2014 Materials as stem cell regulators *Nat. Mater.* **13** 547–57
[9] Teng Y D, Lavik E B, Qu X, Park K I, Ourednik J, Zurakowski D, Langer R, Snyder E Y 2002 Functional recovery following traumatic spinal cord injury mediated by a unique polymer scaffold seeded with neural stem cells *Proc. Natl Acad. Sci. USA* **99** 3024–9
[10] Carlberg, B, Axell M Z, Nannmark U, Liu J and Kuhn H G 2009 Electrospun polyurethane scaffolds for proliferation and neuronal differentiation of human embryonic stem cells *Biomed. Mater.* **4** 045004
[11] Sensenig R, Sapir Y, MacDonald C, Cohen S and Polyak B 2012 Magnetic nanoparticle-based approaches to locally target therapy and enhance tissue regeneration *in vivo Nanomedicine* **7** 1425–42
[12] Kim J J, Singh R K, Seo S J, Kim T H, Kim J H, Lee E J and Kim H W 2014 Magnetic scaffolds of polycaprolactone with functionalized magnetite nanoparticles: physicochemical, mechanical, and biological properties effective for bone regeneration *RSC Adv.* **4** 17325–36
[13] Bock N, Riminucci A, Dionigi C, Russo A, Tampieri A, Landi E, Goranov V A, Mrcacci M and Dediu V 2010 A novel route in bone tissue engineering: magnetic biomimetic scaffolds *Acta Biomater.* **6** 786–96
[14] Yamamoto Y, Ito A, Kato M, Kawabe Y, Shimizu K, Fujita H, Nagamori E and Kamihira M 2009 Preparation of artificial skeletal muscle tissues by a magnetic force-based tissue engineering technique *J. Biosci. Bioeng.* **108** 538–43
[15] Petri D F S 2015 Xanthan gum: a versatile biopolymer for biomedical and technological applications *J. Appl. Polym. Sci.* **132** 42035
[16] Reddy N and Yang Y Q 2010 Citric acid cross-linking of starch films *Food Chem.* **118** 702–11
[17] Bueno V B, Bentini R, Catalani L H and Petri D F 2013 Synthesis and swelling behavior of xanthan-based hydrogels *Carbohydr. Polym.* **92** 1091–9
[18] Bueno V B and Petri D F 2014 Xanthan hydrogel films: molecular conformation, charge density and protein carriers *Carbohydr. Polym.* **101** 897–904
[19] Bueno V B, Bentini R, Catalani L H, Barbosa L R and Petri D F S 2014 Synthesis and characterization of xanthan–hydroxyapatite nanocomposites for cellular uptake *Mater. Sci. Eng.* C **37** 195–203
[20] Bueno V B, Silva A M, Barbosa L R, Catalani L H, Teixeira-Neto E, Cornejo D R and Petri D F S 2013 Hybrid composites of xanthan and magnetic nanoparticles for cellular uptake *Chem. Commun.* **49** 9911–13
[21] Hooper M, Hardy K, Handyside A, Hunter S and Monk M 1987 HPRT-deficient (Lesch-Nyhan) mouse embryos derived from germline colonization by cultured cells *Nature* **326** 292–5
[22] Fornazari M, Nascimento I C, Nery A A, da Silva C C, Kowaltowski A J and Ulrich H 2011 Neuronal differentiation involves a shift from glucose oxidation to fermentation *J. Bioenerg. Biomembr.* **43** 531–9
[23] Strober W 2001 Trypan blue exclusion test of cell viability *Curr. Protoc. Immunol.* **21** A.3B.1–2
[24] Glaser T, de Oliveira S L, Cheffer A, Beco R, Martins P, Fornazari M, Lameu C, Costa H M Jr, Coutinho-Silva R and Ulrich H 2014 Modulation of mouse embryonic stem cell proliferation and neural differentiation by the P2X7 receptor *PLoS One* **9** e96281
[25] Lei L, Ling-Ling J, Yun Z and Gang L 2013 Toxicity of superparamagnetic iron oxide nanoparticles: Research strategies and implications for nanomedicin *Chin. Phys.* B **22** 127503
[26] Xu H and Gu N 2014 Magnetic responsive scaffolds and magnetic fields in bone repair and regeneration *Frontiers Mater. Sci.* **8** 20–31
[27] Yu D, Neeley W L, Pritchard C D, Slotkin J R, Woodard E J, Langer R, Teng Y D 2009 Blockade of peroxynitrite-induced neural stem cell death in the acutely injuried spinal cord by drug-releasing polymer *Stem Cell* **27** 1212–22
[28] Dobson J. 2001 Nanoscale biogenic iron oxides and neurodegenerative disease *FEBS Lett.* **496** 1–5
[29] Kirschvink J L. Kobayashi-Kirschvink A and Woodford B J 1992 Magnetite biomineralization in the human brain *Proc. Natl Acad. Sci. USA* **89** 7683–7
[30] Dadras A, Riazi G H, Afrasiabi A, Naghshineh A, Ghalandari B and Mokhtari F 2013 *In vitro* study on the alterations of brain tubulin structure and assembly affected by magnetite nanoparticles *J. Biol. Inorg. Chem.* **18** 357–69